Calcineurin, the Ca^{2+}-dependent phosphatase, regulates Rga2, a Cdc42 GTPase-activating protein, to modulate pheromone signaling

Nina Ly and Martha S. Cyert*
Department of Biology, Stanford University, Stanford, CA 94305

ABSTRACT **Calcineurin, the conserved Ca^{2+}/calmodulin-activated phosphatase, is required for viability during prolonged exposure to pheromone and acts through multiple substrates to down-regulate yeast pheromone signaling. Calcineurin regulates Dig2 and Rod1/Art4 to inhibit mating-induced gene expression and activate receptor internalization, respectively. Recent systematic approaches identified Rga2, a GTPase-activating protein (GAP) for the Cdc42 Rho-type GTPase, as a calcineurin substrate. Here we establish a physiological context for this regulation and show that calcineurin dephosphorylates and positively regulates Rga2 during pheromone signaling. Mating factor activates the Fus3/MAPK kinase, whose substrates induce gene expression, cell cycle arrest, and formation of the mating projection. Our studies demonstrate that Fus3 also phosphorylates Rga2 at inhibitory S/TP sites, which are targeted by Cdks during the cell cycle, and that calcineurin opposes Fus3 to activate Rga2 and decrease Cdc42 signaling. Yeast expressing an Rga2 mutant that is defective for regulation by calcineurin display increased gene expression in response to pheromone. This work is the first to identify cross-talk between Ca^{2+}/calcineurin and Cdc42 signaling and to demonstrate modulation of Cdc42 activity through a GAP during mating.**

Monitoring Editor
Daniel J. Lew
Duke University

Received: Jun 16, 2016
Revised: Jan 4, 2017
Accepted: Jan 4, 2017

INTRODUCTION

Calcineurin (CN), the Ca^{2+}/calmodulin-activated phosphatase, translates Ca^{2+} signals into downstream regulatory events and is widely expressed in the animal and fungal kingdoms (Rusnak and Mertz, 2000). Although CN structure is highly conserved, its physiological functions have diverged significantly in fungi and mammals due to rapid rewiring of the CN signaling network through gain and loss of docking motifs in its substrates (Goldman *et al.*, 2014). In mammals, CN is best known as the target of immunosuppressant drugs cyclosporin A and FK506, which inhibit CN-mediated dephosphorylation of NFAT transcription factors to block T-cell activation (Crabtree and Schreiber, 2009). In fungi, CN broadly regulates stress responses and is essential under stringent growth conditions (Cyert and Philpott, 2013). These include survival in a mammalian host for several pathogenic fungi, where CN is required for virulence (Juvvadi *et al.*, 2014). Thus elucidation of fungal CN signaling pathways may identify novel targets for antifungal drug development.

In the budding yeast *Saccharomyces cerevisiae*, CN is dispensable for growth under standard laboratory conditions, when cytosolic Ca^{2+} levels are low, but essential under conditions that trigger Ca^{2+} signaling, that is, environmental stress, including ionic and cell wall stress, and pheromone signaling (Cyert and Philpott, 2013, Carbó *et al.*, 2017). CN regulates distinct substrates and processes under different signaling conditions (Cyert and Philpott, 2013; Goldman *et al.*, 2014; Arsenault *et al.*, 2015; Guiney *et al.*, 2015). In cells responding to pheromone, CN inhibits mating-induced gene expression and reduces levels of pheromone receptor at the cell surface by dephosphorylating Dig2 and Rod1/Art4, respectively (Cyert and Thorner, 1992; Alvaro *et al.*, 2014, 2016; Goldman *et al.*, 2014). This CN-mediated down-regulation of the pheromone response is essential because CN mutants lose viability during prolonged exposure to mating pheromone (Moser *et al.*, 1996; Withee *et al.*, 1997). A systematic screen uncovered >15 proteins and their associated processes as novel targets of CN (Goldman *et al.*, 2014). One of these, Rga2, a GTPase-activating protein (GAP) for the Rho-type

This article was published online ahead of print in MBoC in Press (http://www.molbiolcell.org/cgi/doi/10.1091/mbc.E16-06-0432) on January 11, 2017.

*Address correspondence to: Martha S. Cyert (mcyert@stanford.edu).

Abbreviations used: Cdk, cyclin-dependent kinase; CN, calcineurin; GAP, GTPase-activating protein; GEF, guanine nucleotide exchange factor; MAPK, mitogen-activated protein kinase.

GTPase Cdc42, suggested previously undescribed cross-talk between CN and Cdc42 signaling and was chosen for further investigation. Specifically, we sought to identify the effect of CN-dependent dephosphorylation on Rga2 function and the physiological context in which this regulation occurs.

Members of the Rho family of small GTPases, that is, Rho, Rac, and Cdc42, are master regulators that transduce extracellular signals into complex behaviors such as wound healing and chemotaxis by coordinately regulating cytoskeletal dynamics, vesicle trafficking, gene expression, and proliferation (Hall, 2012; Abreu-Blanco *et al.*, 2014; Mócsai *et al.*, 2015). Rho GTPases control diverse effectors and act as molecular switches; the active, GTP-bound state is promoted by guanine nucleotide exchange factors (GEFs) and inactivation is mediated by GAPs, which stimulate conversion to GDP-bound Rho (Hall, 2012). These Rho GEFs and GAPs allow Rho GTPase signaling to be regulated in a tissue- and signal-specific manner and precisely control the spatiotemporal pattern of Rho GTPase cycling in vivo (Fritz and Pertz, 2016). Perturbation of Rho GAPs causes pathologies including cancer, mental retardation, and kidney disease (Cherfils, 2014), and understanding their regulation provides critical insight into the complex control of Rho GTPase signaling in vivo (Bernards and Settleman, 2004).

In *S. cerevisiae*, the conserved Cdc42 GTPase is essential for asymmetric cell growth and critically regulates responses to pheromone, nutrient limitation, and osmotic stress (Chen and Thorner, 2007; Bi and Park, 2012). Cdc42 activity is controlled by a single essential GEF, Cdc24, and multiple GAPs, Bem3, Rga1, and Rga2 (Zheng *et al.*, 1993, 1994; Stevenson *et al.*, 1995; Chen *et al.*, 1996; Smith *et al.*, 2002), which serve both overlapping and unique functions (Smith *et al.*, 2002; Caviston *et al.*, 2003; Tong *et al.*, 2007). Bem3 and Rga2 undergo cell cycle–dependent phosphorylation (Knaus *et al.*, 2007; McCusker *et al.*, 2007; Sopko *et al.*, 2007), and cyclin-dependent kinases (Cdks) target inhibitory S/TP sites in Rga2 to facilitate activation of Cdc42 during bud emergence in G1 (Sopko *et al.*, 2007). During mating, pheromone-activated receptor recruits Cdc24 to the membrane, causing a local increase in Cdc42-GTP, which initiates a kinase cascade that culminates in activation of the Fus3 mitogen-activated protein kinase (MAPK) to induce cell cycle arrest, gene expression, and shmoo formation (Alvaro and Thorner, 2016). Although deletion of Cdc42 GAPs elevates both basal and induced levels of pheromone-dependent gene expression, whether these proteins are regulated during the mating response has not been investigated (Smith *et al.*, 2002).

In this work, we uncover a new role for Rga2 in regulating Cdc42 activity during pheromone signaling. Rga2 is phosphorylated by Fus3 on inhibitory S/TP sites and dephosphorylated by CN to dampen pheromone signaling. When exposed to mating factor, cells expressing an Rga2 mutant deficient for CN-dependent regulation show increased mating-induced gene expression. Thus we establish a novel mechanism, mediated by Ca^{2+} and CN, that regulates Cdc42 signaling, and identify Rga2 as an additional target through which calcineurin limits the pheromone response.

RESULTS AND DISCUSSION

CN interacts with and positively regulates Rga2 in vivo

Previous work showed that CN dephosphorylates Rga2 in vitro and in addition identified a sequence that lies downstream of the N-terminal LIM domains, PQVLVS (amino acids 192–197), as matching the consensus for a known CN-docking motif termed PxIxIT (Figure 1A; Roy *et al.*, 2007; Goldman *et al.*, 2014). To examine the interaction of Rga2 with CN, we first showed that, when fused to glutathione *S*-transferase (GST), a 22–amino acid sequence from Rga2 containing PQVLVS copurified with recombinant hexahistidine (6xHis)-CN and that, consistent with PxIxIT-dependent binding, mutation of key residues to alanine (AQALAA) disrupted the interaction (Figure 1B). To determine whether this putative PxIxIT site is functional in the context of the full-length protein, we expressed wild-type (WT) Rga2 ($Rga2^{WT}$) or PxIxIT mutants ($Rga2^{AQALAA}$ or a deletion of PQVLVS, $Rga2^{P\Delta}$) in *Escherichia coli* and tested them for copurification with GST-CN. $Rga2^{WT}$ but not $Rga2^{AQALAA}$ or $Rga2^{P\Delta}$ copurified with GST-CN, and none of the Rga2 proteins copurified with GST (Figure 1C). Thus the PQVLVS sequence mediates a specific interaction with CN. To examine whether, as for other substrates (Grigoriu *et al.*, 2013; Alvaro *et al.*, 2014; Goldman *et al.*, 2014; Arsenault *et al.*, 2015; Guiney *et al.*, 2015), CN fails to regulate Rga2 PxIxIT mutants, we examined the electrophoretic mobility of Rga2 in extracts of yeast in which CN was acutely activated by addition of 200 mM $CaCl_2$. A fast-migrating form of Rga2 was observed, whereas an additional, slower-migrating band appeared in cultures that were pretreated with the CN inhibitor FK506 (Figure 1D). Consistent with previous findings, this slower-migrating band reflects hyperphosphorylation (Sopko *et al.*, 2007; Goldman *et al.*, 2014) and confirms that Rga2 is dephosphorylated by CN in vivo. In contrast to $Rga2^{WT}$, the Rga2 PxIxIT mutants $Rga2^{AQALAA}$ and $Rga2^{P\Delta}$ were hyperphosphorylated under CN activating conditions, and phosphorylation levels were unaffected by FK506, demonstrating the abrogation of CN-dependent dephosphorylation. Thus Rga2 PxIxIT mutants allow us to investigate the functional consequences of CN-mediated regulation of Rga2.

Because Cdc42 GAPs are functionally redundant, we examined Rga2 activity in a strain lacking three Cdc42 GAPs (*bem3*Δ *rga1*Δ *rga2*Δ), which displays elevated levels of pheromone-induced gene expression (Smith *et al.*, 2002). In the presence of pheromone, high levels of *FUS1*-LacZ activity were observed in cells overexpressing vector or catalytically inactive Rga2 (K872A, $Rga2^{GAPmut}$), which were reduced in cells overexpressing $Rga2^{WT}$ (Figure 1E). In comparison, neither of the Rga2 PxIxIT mutants was as effective as $Rga2^{WT}$ at reducing β-galactosidase activity ($p < 0.01$ and $p < 0.05$, Figure 1E), despite equivalent expression levels for all Rga2 variants (unpublished data). As a second measure of function, Rga2 was overexpressed in wild-type cells. As previously observed, overexpression of $Rga2^{WT}$, but not $Rga2^{GAPmut}$ or vector, decreased the growth rate (Figure 1F; Sopko *et al.* 2007). In contrast, neither of the Rga2 PxIxIT mutants slowed growth to the same degree as $Rga2^{WT}$ ($p < 0.001$, Figure 1F). Together these findings show that loss of regulation by CN decreases Rga2 function in vivo and suggest that CN activates Rga2, presumably through dephosphorylation.

CN opposes Fus3 to regulate Rga2 during pheromone signaling

To determine when CN dephosphorylates Rga2 in vivo, we sought physiological conditions under which the phosphorylation status of $Rga2^{WT}$ and $Rga2^{AQALAA}$ differs (as in Figure 1D). Rga2 is expressed at very low levels from its native promoter (200–300 molecules/cell; Ghaemmaghami *et al.*, 2003) and could not be reliably detected by immunoblot. Therefore we expressed FLAG-tagged Rga2 from a CEN plasmid under control of the GAL promoter in a wild-type strain (*BEM3 RGA1 RGA2*) carrying the GEV chimera for β-estradiol–induced expression of galactose-regulated genes (Gao and Pinkham, 2000; Veatch *et al.*, 2009). Cells were grown in the presence of low β-estradiol levels to allow detection of Rga2 without perturbing cell growth (Supplemental Figure S1, A and B). During G1 phase of the cell cycle, Cdks phosphorylate and inhibit Rga2, maximizing Cdc42 activation for bud emergence (Sopko *et al.*, 2007).

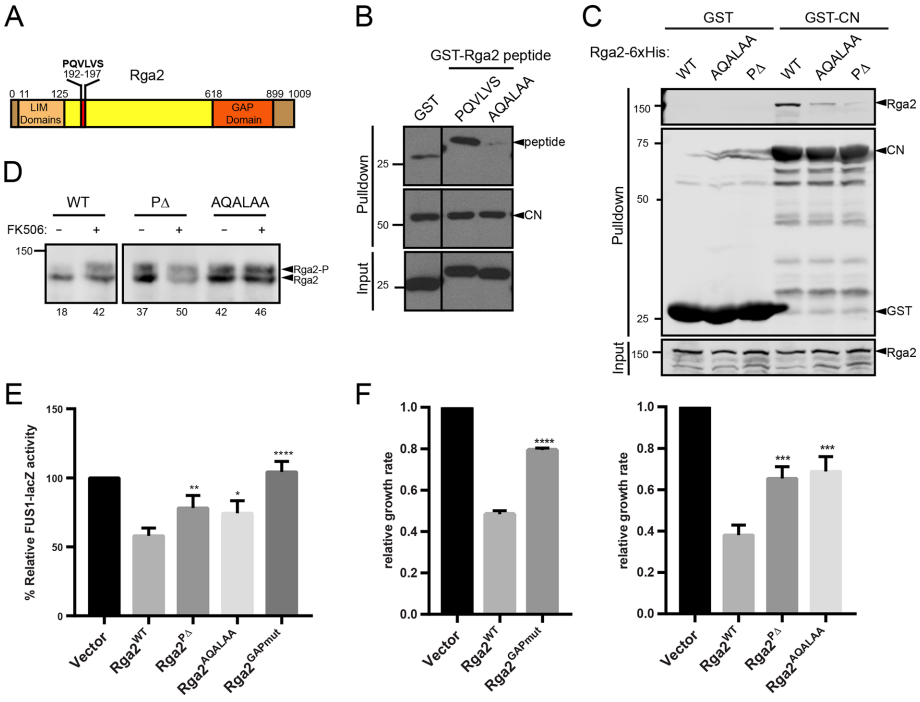

FIGURE 1: PQVLVS sequence binds CN and is required for regulation of Rga2 by CN. (A) The domain structure of Rga2 and position of the PQVLVS sequence. (B) Immunoblots showing that GST fused to amino acids 184–205 from Rga2, which contains PQVLVS, copurifies with 6xHis-CN, whereas the mutated sequence GST-AQALAA and GST do not (Pulldown). Arrowheads, positions of CN (anti-His) and GST-peptide fusion protein (anti-GST). Input, immunoblot (anti-GST) showing amounts of GST proteins added to each assay. (C) Immunoblot showing that recombinant 6xHis-Rga2^{WT} copurifies with GST-CN but not with PxIxIT mutants Rga2^{AQALAA} or Rga2$^{P\Delta}$, with residues 192–197 deleted (Pulldown). Arrowheads, positions of Rga2 (anti-His), GST-CN, and GST (anti-GST). Input, immunoblot (anti-His) showing amounts of Rga2 proteins added to each assay. (D) Calcineurin dephosphorylates Rga2 in vivo under Ca^{2+}-activating conditions. Cells (BY263) expressing Rga2-FLAG plasmids were treated with CN inhibitor FK506 or vehicle before 200 mM $CaCl_2$ activation of CN. Arrowheads, hyperphosphorylated (Rga2-P) and hypophosphorylated (Rga2) forms (anti-FLAG). Percentage of total Rga2 signal represented by slower-migrating band is shown below each lane. (E, F) Rga2 PxIxIT mutants are less active in vivo than Rga2^{WT}. (E) Yeast lacking Cdc42 GAPs (*bem3*Δ *rga1*Δ *rga2*Δ) and containing a pheromone-responsive *FUS1-LacZ* reporter were incubated with pheromone before measurement of β-galactosidase activity. Strains also expressed pGAL1-FLAG vector or Rga2-FLAG plasmids as indicated. Error bars are SD from four biological replicates. (F) Growth rate (doublings/hour) of WT yeast (NLY33) treated with 20 μM estradiol and expressing pEG(KT) vector or GST-Rga2 plasmids. Error bars are SD from three biological replicates. For E and F, all values were normalized to vector, and statistical difference from Rga2^{WT} was assessed using one-way ANOVA with Tukey's correction for multiple comparisons, *$p < 0.05$, **$p < 0.01$, ***$p < 0.001$, ****$p < 0.0001$.

The phosphatase(s) that counteract these phosphorylation events have not been identified. Because CN opposes Cdk1 regulation of the S-phase transcription factor Hcm1 (Arsenault *et al.*, 2015), we tested whether CN dephosphorylates Rga2 during the cell cycle. Yeast cells synchronized in G1 by pheromone arrest were released into the cell cycle, and the electrophoretic mobility of Rga2^{WT} and Rga2^{AQALAA} were compared. Rga2^{WT} ran as a doublet, and the relative abundance of the upper band varied through the cell cycle, peaking at 30–45 min, which coincided with S phase (Supplemental Figure S1, B and C). This agrees with previous studies, which demonstrated that hyperphosphorylation of Rga2 by G1-Cdks results in its decreased electrophoretic mobility (Sopko *et al.*, 2007). Rga2^{AQALAA} was indistinguishable from Rga2^{WT} in these analyses, suggesting that CN does not dephosphorylate Rga2 during the mitotic cell cycle. Of interest, PxIxIT-dependent effects on growth inhibition were observed when Rga2 was overexpressed (Figure 1F), indicating possible activation of CN under these conditions.

While executing these cell cycle studies, we observed that the relative abundance of the upper band in the doublet differed strikingly between Rga2^{WT} and Rga2^{AQALAA} in extracts of pheromone-arrested cells. Under these conditions, ~70% of Rga2^{AQALAA} appeared as the slower-migrating form, whereas, consistent with CN-dependent dephosphorylation, the majority of Rga2^{WT} was in the faster-migrating form (Figure 2A). To confirm that these electrophoretic mobility differences were due to phosphorylation, we purified Rga2^{WT} and Rga2^{AQALAA} from pheromone-treated cells and incubated them with nonspecific λ-phosphatase in the presence or absence of phosphatase inhibitors. Phosphatase treatment of either Rga2^{WT} or Rga2^{AQALAA} increased the abundance of the faster-migrating band, and abrogation of this shift by phosphatase inhibitors confirmed that it was caused by dephosphorylation (Figure 2B).

Next we investigated the identity of the kinase that phosphorylates Rga2 during pheromone signaling. The Fus3 MAPK was a prime candidate because it is activated during pheromone signaling and, like Cdks, targets S/TP sites. To test for Fus3-dependent phosphorylation of Rga2 in vivo, we incubated cells expressing an analogue-sensitive allele of Fus3 (Fus3-as1; Bishop *et al.*, 2000; Matheos *et al.*, 2004) with pheromone. Ten minutes after addition of inhibitor, Rga2 phosphorylation was reduced compared with cells treated with vehicle (Figure 2C), suggesting that Fus3 phosphorylates Rga2 during pheromone signaling. In vitro, recombinant WT Fus3 (Fus3^{WT}) but not the kinase-dead form (Fus3^{K42R}; Parnell *et al.*, 2005) directly phosphorylated Rga2^{WT} and Rga2^{AQALAA} to similar degrees, confirming that differences in their phosphorylation states observed in vivo are due to differential dephosphorylation rather than phosphorylation (Figure 2D). Together these results newly identify Rga2 as a direct Fus3 substrate during the pheromone response.

To test whether Fus3 regulates similar sites as Cdks on Rga2, we used an Rga2 mutant in which eight experimentally verified Cdk-phosphorylated residues were changed to alanine (Rga2^{8A}; Sopko *et al.* 2007). Phosphorylation of Rga2^{8A} by Fus3 was drastically reduced in vivo and in vitro, suggesting that it targets one or more of the same sites as Cdks (Figure 2, E and F). Previous work established that phosphorylation of these sites by Cdks inhibits Rga2 function, thereby increasing active Cdc42 levels and promoting bud emergence; overexpression of a nonphosphorylatable mutant decreases Cdc42-GTP levels in vivo and causes accumulation of large, unbudded cells arrested in G1 (Sopko *et al.*, 2007). Therefore phosphorylation of these sites by Fus3 strongly suggests that it similarly inhibits Rga2 during the pheromone response, when Cdk signaling is

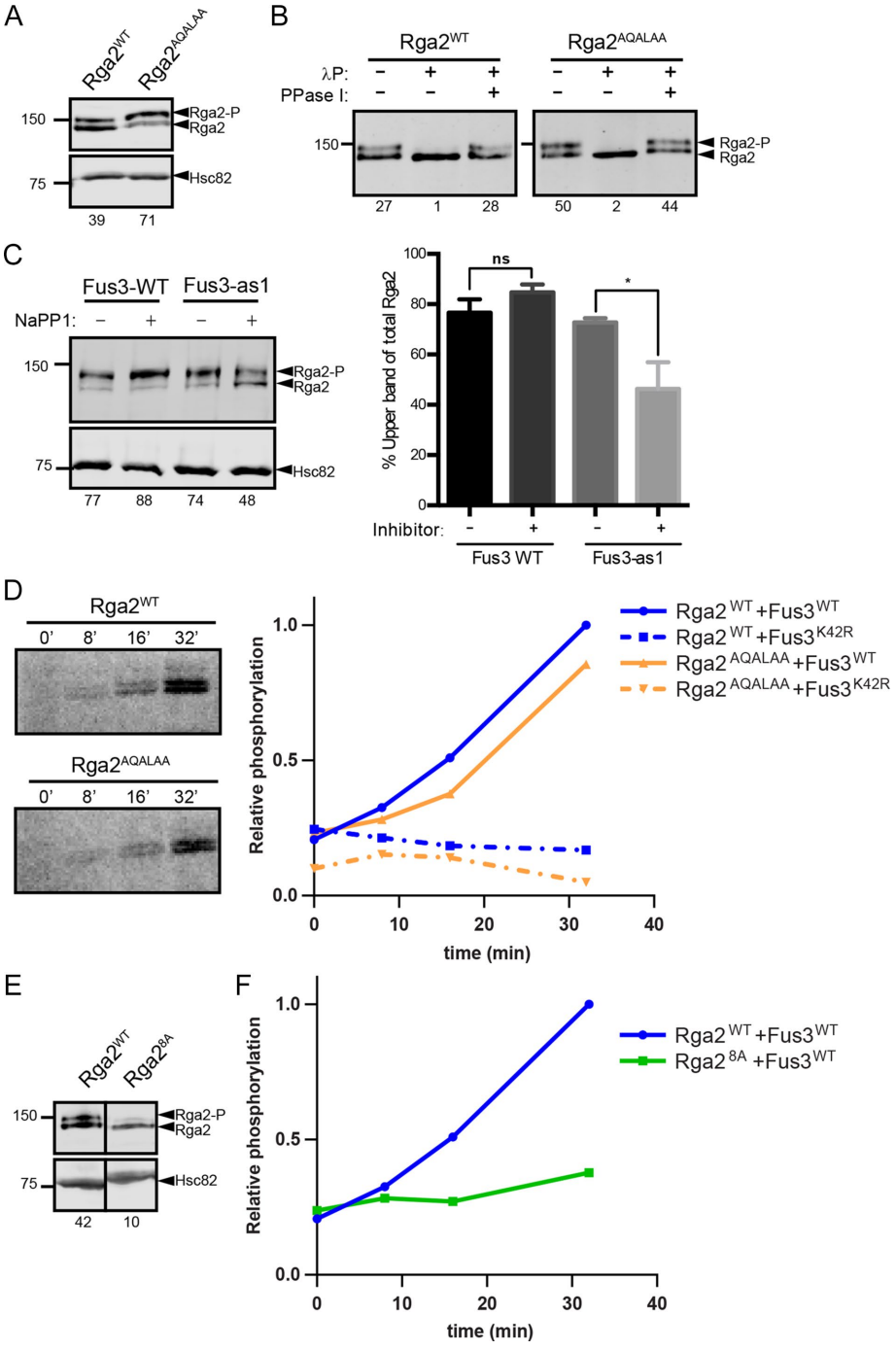

FIGURE 2: Fus3-dependent phosphorylation of Rga2 during pheromone arrest. (A) Immunoblot showing enrichment of slow-migrating Rga2-FLAG band in extracts of pheromone-treated cells expressing $Rga2^{AQALAA}$ as compared with $Rga2^{WT}$. (B) Shift in electrophoretic mobility is due to phosphorylation. $Rga2^{WT}$ or $Rga2^{AQALAA}$ was immunopurified from pheromone-treated cells, treated with λ-phosphatase (λP) in the presence or absence of phosphatase inhibitors (PPase I), and analyzed by immunoblot (anti-FLAG). (C) Rga2 phosphorylation in pheromone-treated cells is dependent on Fus3. Fus3-WT (NLY39 + MR4937) or Fus3-as1 (NLY39 + MR4938) cells expressing $Rga2^{WT}$-FLAG were treated with or without 1Na-PP1 inhibitor. Representative blot shows Rga2 electrophoretic mobility (anti-FLAG). Graph shows quantification and SD from three biological replicates, $*p < 0.05$, Student's *t* test. (D) Rga2 is a substrate for Fus3 in vitro. Recombinant 6xHis-Rga2 and $Fus3^{WT}$ (solid line) or kinase-dead $Fus3^{K42R}$ (dashed line) were incubated with [γ-^{32}P]ATP-, and ^{32}P incorporation at 0, 8, 16, and 32 min was quantified by phosphoimager analysis. The ^{32}P signal was adjusted for Rga2 protein level, normalized to maximal signal for $Rga2^{WT}$, and relative phosphorylation level is displayed. (E, F) Fus3 and CDKs regulate similar phosphosites on Rga2. (E) During pheromone signaling, $Rga2^{8A}$ is a poor substrate in vivo. Cells (NLY33) transformed with Rga2-FLAG plasmids were induced with 5 nM estradiol and incubated with 10 μM αF. (F) $Rga2^{8A}$ phosphomutant is a poor substrate for Fus3 in vitro. Recombinant 6xHis-$Rga2^{8A}$ and $Fus3^{WT}$ were incubated with [γ-^{32}P]ATP, and ^{32}P incorporation at 0, 8, 16, and 32 min was quantified as described in D. For A–C and E, phosphorylation was assayed by electrophoretic mobility, with arrowheads indicating hyperphosphorylated (Rga2-P) and hypophosphorylated (Rga2) forms (anti-FLAG) and Hsc82 (anti-Hsc82) loading control. Percentage of total Rga2 signal represented by slower-migrating band is shown below each lane.

inhibited, to promote the sustained activation of Cdc42 required for downstream signaling events, that is, cell cycle arrest, expression of mating genes, and shmoo formation (Alvaro and Thorner, 2016). In contrast, we predict that, by dephosphorylating Rga2, CN down-regulates Cdc42 and pheromone signaling.

Under maximal signaling conditions, CN positively regulates Rga2 to suppress the pheromone response

Next we examined the timing of Rga2 dephosphorylation by CN during the pheromone response. The electrophoretic mobility of $Rga2^{WT}$ and $Rga2^{AQALAA}$ (expressed at low levels as in Supplemental Figure S1) were compared in extracts of WT cells (*BEM3 RGA1 RGA2)* that were synchronized by release from hydroxyurea (HU)-triggered S-phase arrest and stimulated with mating factor before G1 ($t = 0$; Figure 3A). Dephosphorylation of $Rga2^{WT}$ was detected 30 min after pheromone addition, which coincided with entry into G1, the onset of pheromone signaling as detected by the appearance of active Fus3 (Fus3-P) and initial appearance of cells exhibiting early shmoo morphology (Figure 3, A–D). Compared to $Rga2^{WT}$, $Rga2^{AQALAA}$ remained hyperphosphorylated throughout the time course, suggesting that CN was activated early and throughout the pheromone response to regulate Rga2 (Figure 3D). Consistent with this idea, studies of single yeast cells exposed to pheromone revealed that intracellular Ca^{2+} spikes initiate early during pheromone signaling and persist throughout the response, with the frequency and total number of Ca^{2+} signals increasing as a function of pheromone concentration (Carbó *et al.*, 2017). However, these Ca^{2+} signals are asynchronous and heterogeneous in amplitude and duration, suggesting that each time point of our experiment included a variable subset of cells that were undergoing Ca^{2+}/CN-activated

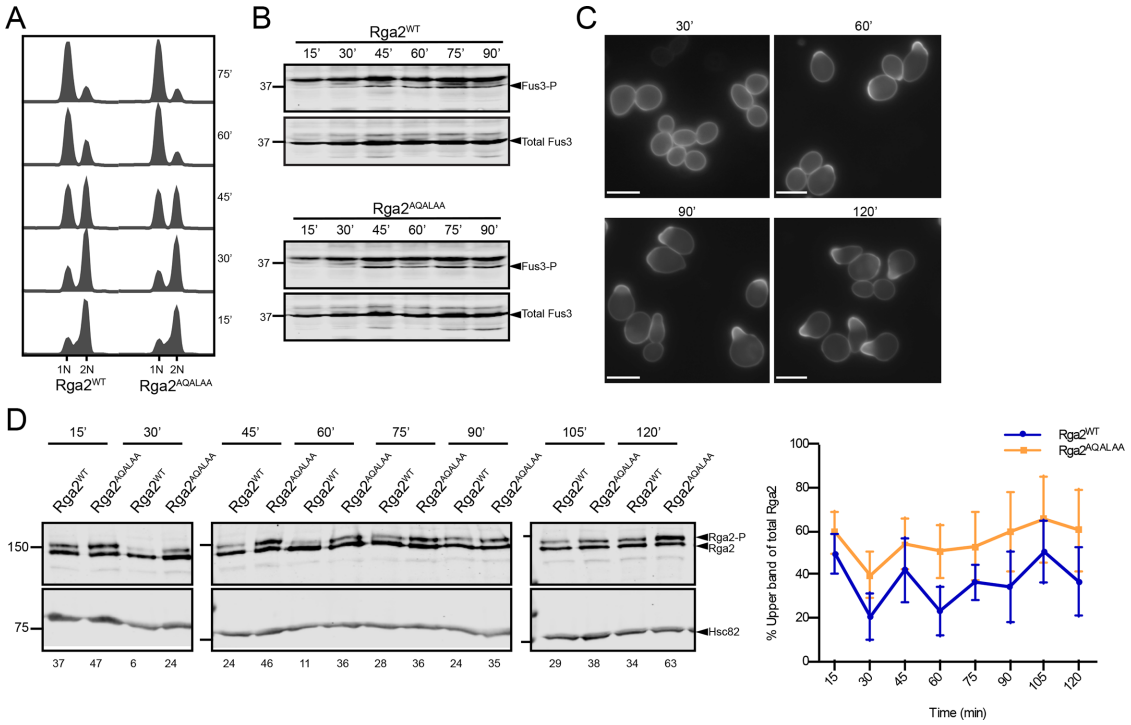

FIGURE 3: CN regulates Rga2 throughout the pheromone response. Analysis of yeast (NLY33) synchronized at S-phase with HU and then released; addition of 5 μM αF occurred at time 0, and samples were removed every 15 min thereafter. Strains expressed either Rga2^{WT} (pBA2059) or Rga2^{AQALAA} (pNL111) induced with 5 nM estradiol. (A) FACS analysis shows progressive arrest in G1. (B) Immunoblots show accumulation of active Fus3 (Fus3-P, anti-p44/42 MAPK) and total Fus3 (anti-Fus3). (C) Representative images of Rga2^{WT} cells stained with FITC-concanavalin A at indicated times show progressive accumulation of shmoo morphology. Scale bar, 5 μm. (D) Representative blot of Rga2^{WT} and Rga2^{AQALAA} phosphorylation state. Arrowheads, hyperphosphorylated (Rga2-P) and hypophosphorylated (Rga2) forms (anti-FLAG) and Hsc82 loading control (anti-Hsc82). Percentage of total Rga2 signal represented by slower-migrating band is shown below each lane, and results from four biological replicates are quantified in the graph to the right, with error bars represented as SD. Rga2^{AQALAA} differs from Rga2^{WT}, $p < 0.01$, Wilcoxon paired nonparametric test. Refer to Supplemental Figure S1D for quantification of each biological replicate.

dephosphorylation of Rga2. Thus, in four independent experiments, we consistently observed that Rga2^{AQALAA} was hyperphosphorylated compared with Rga2^{WT} throughout the pheromone response, although the extent of hyperphosphorylation observed at each time point varied (Figure 3D and Supplemental Figure S1D, $p < 0.01$). Together these observations indicate that high levels of pheromone trigger Ca^{2+} signals that activate CN and suggest that CN and Fus3 oppose each other in regulating Rga2. By positively regulating Rga2, CN may inhibit the ability of Cdc42 to regulate cell morphology, cell cycle arrest, and/or gene transcription in response to pheromone (Alvaro and Thorner, 2016).

To assess the phenotypic consequences of Rga2 dephosphorylation, we constructed isogenic strains that contained all Cdc42 GAPs and differed only in the susceptibility of Rga2 to CN-mediated dephosphorylation. Replacement of genomic *RGA2* through integration of isogenic, tagged *RGA2*^{WT} or *RGA2*^{AQALAA} alleles at the endogenous locus allowed for their expression at physiological levels. Characterization of these integrated Rga2^{WT} or Rga2^{AQALAA} strains through the pheromone response showed no detectable differences in the timing of cell cycle arrest and shmoo formation (Supplemental Figure S2, A and B) or in shmoo morphology (unpublished data). To test whether CN regulates pheromone-induced gene expression through Rga2, we assayed *FUS1*-LacZ activity in cells treated with a range of mating factor concentrations. Although Rga2^{WT} and Rga2^{AQALAA} responded similarly to low pheromone concentrations, there was a reproducible and statistically significant difference at higher pheromone concentrations (>5 μM), with Rga2^{AQALAA} cells exhibiting higher levels of β-galactosidase activity than Rga2^{WT} (Figure 4A, $p < 0.01$ and $p < 0.05$). This difference between Rga2^{WT} and Rga2^{AQALAA} was consistent, as additional assays with a larger sample size (n ≥ 15) showed increased statistical significance (Figure 4B, $p < 0.0001$ at 5 and 10 μM mating factor). Thus, under conditions of sustained pheromone signaling, which trigger Ca^{2+} bursts, CN activates Rga2 to decrease pheromone-induced gene expression.

Cdc42 signaling is regulated through its GAP, Rga2, during pheromone signaling

The yeast response to pheromone has been intensively studied and yet continues to yield new insights into the fundamental regulatory features of signaling pathways. Our findings provide the first evidence that a Rho GTPase-activating protein, Rga2, modulates the output of this response and is antagonistically regulated by Fus3, the pheromone-activated MAPK, and CN, the Ca^{2+}-activated phosphatase (Figure 5A).

During mating, Fus3 substrates induce cell cycle arrest, gene expression, actin polarization and cell fusion (Alvaro and Thorner, 2016). Fus3 promotes polarization by phosphorylating the Bni1 formin, which is also an effector of Cdc42 (Elion *et al.*, 1993; Tedford *et al.*, 1997; Matheos *et al.*, 2004). Therefore our finding that Fus3 regulates Rga2 suggests that this MAPK elevates Cdc42 signaling to create positive feedback that reinforces activation of

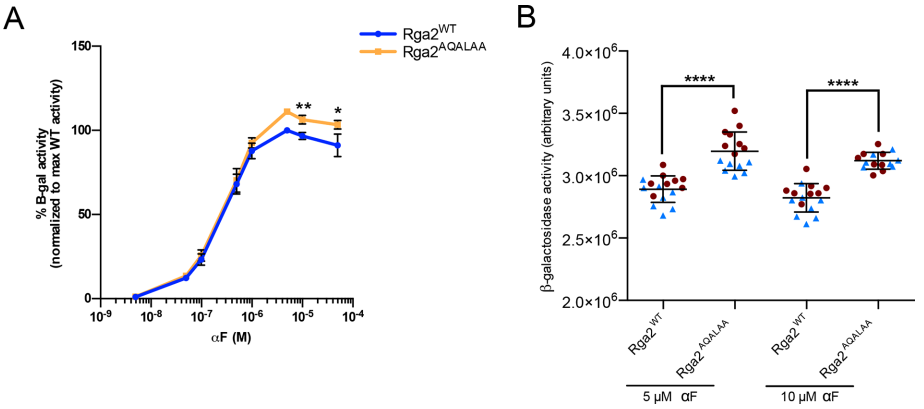

FIGURE 4: CN regulates Rga2 to oppose pheromone signaling. (A) Rga2^{AQALAA} yeast cells, compared with Rga2^{WT}, are more sensitive to high pheromone concentrations. Integrated Rga2 alleles (WT, NLY52; AQALAA, NLY54) were assayed for FUS1-lacZ activity after treatment with pheromone at indicated concentrations. FUS1-lacZ activity was normalized to maximum Rga2^{WT} value occurring at 5 μM to represent relative levels. Error bars represent SD from four biological replicates. *$p < 0.05$, **$p < 0.01$. Values statistically significant from Rga2^{WT} were assessed using Student's *t* test. (B) Yeast expressing Rga2^{AQALAA} display higher levels of pheromone-induced FUS1-lacZ activity. Cells were treated with 5 or 10 μM αF as indicated. Statistical significance assessed by Student's *t* test with $n = 16$ biological samples for Rga2^{WT} and $n = 15$ for Rga2^{AQALAA}, performed over 2 d (blue triangles, day 1; red circles, day 2). Middle bar represents mean with errors bars as SD, ****$p < 0.0001$.

Bni1 and of Fus3 itself, which is stimulated in a Cdc42-dependent manner.

The CN signaling network is essential for survival of yeast cells during prolonged exposure to high concentrations of pheromone and acts through multiple substrates to down-regulate signaling. Previous studies established that CN dephosphorylates and activates Dig2, an inhibitor of Ste12, to reduce mating-induced gene expression (Figure 5B). CN reverses Fus3-mediated phosphorylation of Dig2, and directly competes with Fus3 at overlapping CN- and MAPK-docking sites for Dig2 binding (Goldman *et al.*, 2014). We speculate that CN signaling substantially decreases mating-induced gene expression through its combined regulation of Rga2 and Dig2. Furthermore, CN reduces signaling by activating Rod1/Art4-mediated receptor endocytosis (Alvaro *et al.*, 2014, 2016) and may dampen other aspects of pheromone signaling through additional substrates. Candidates include the Elm1 kinase, which phosphorylates Gα (GPA1; Clement *et al.*, 2013), proteins associated with polarized growth (Kic1, Boi2, Mlf3; Goldman *et al.*, 2014), and the Crz1 transcription factor, which is activated by CN in response to pheromone (Stathopoulos *et al.*, 1997). Given these multiple points of regulation, it is remarkable that disrupting CN-dependent regulation of a single target, Rga2, in cells that contain multiple Cdc42 GAPs and functional CN substrates noticeably increased pheromone-dependent gene expression.

Although pheromone-induced Ca^{2+} influx is well documented (Iida *et al.*, 1990; Moser *et al.*, 1996; Withee *et al.*, 1997), new studies of Ca^{2+} dynamics in individual yeast cells revealed that pheromone induces asynchronous, heterogeneous Ca^{2+} bursts whose frequency increases with pheromone concentration (Carbó *et al.*, 2017). Consistent with these findings, we observed partial dephosphorylation of Rga2 throughout the pheromone response. Furthermore, we identified increased expression of a mating gene in Rga2^{AQALAA} -expressing cells specifically under maximal

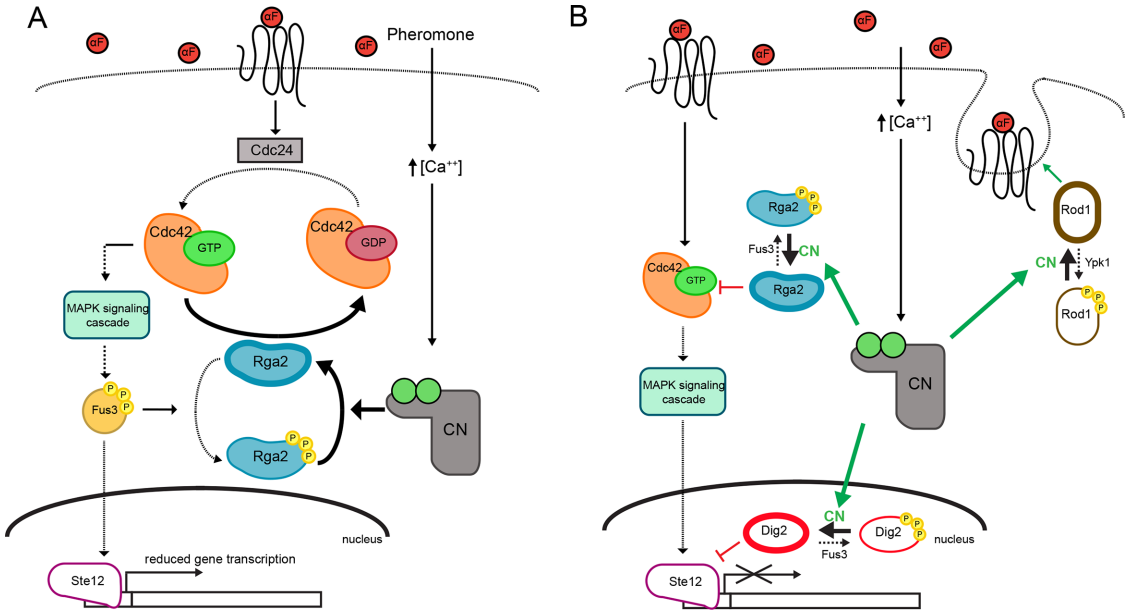

FIGURE 5: Model. (A) In response to high pheromone concentration, Ca^{2+} activates CN, which dephosphorylates and activates Rga2 to reduce Cdc42-GTP levels and MAPK-dependent pheromone signaling. See the text for details. (B) In response to high pheromone concentration, CN inhibits the pheromone response by dephosphorylating an α-arrestin, Rod1/Art4, to promote endocytosis; by dephosphorylating a Cdc42 GAP, Rga2, to down-regulate Cdc42 signaling; and by dephosphorylating a Ste12 inhibitor, Dig2, to inhibit mating-induced gene expression (Alvaro *et al.*, 2014, 2016; Goldman *et al.*, 2014). See the text for details.

pheromone signaling conditions, when Ca^{2+} signaling is most intense. The Ca^{2+}/CN-dependent regulation of pheromone signaling is known only to promote cell survival under conditions of prolonged cell cycle arrest (Withee *et al.*, 1997). However, in many cell types, such as fungal hyphae, pollen tubes, neuronal axons, and mast cells, localized Ca^{2+} gradients regulate Rho GTPase signaling to direct polarized growth and migration (Brand *et al.*, 2014; Sutherland *et al.*, 2014; Chen *et al.*, 2015; Holowka *et al.*, 2016). Thus Ca^{2+}/calcineurin-dependent regulation of Cdc42 signaling may play undiscovered roles in directional aspects of pheromone signaling, such as chemotrophic growth (McClure *et al.*, 2015; Ismael *et al.*, 2016).

Are other Cdc42 GAPs, Rga1 and Bem3, modulated during pheromone signaling? Single deletion or mutation of these GAPs has little or no effect on the pheromone response (Stevenson *et al.*, 1995; Bidlingmaier and Snyder, 2004). Furthermore, Rga2 is the only Cdc42 GAP that harbors a CN-docking site (Goldman *et al.*, 2014) and forms a complex with Cdc24, Bem1, Boi1, and Boi2 (another CN substrate). Proposed to regulate Cdk1-dependent expansion of the yeast cell surface during the cell cycle (McCusker *et al.*, 2007), this complex might also function during pheromone signaling, as most of its components contribute to shmoo formation or localize to the shmoo tip (Chenevert *et al.*, 1992, 1994; Nern and Arkowitz, 1999; Narayanaswamy *et al.*, 2009). Further analyses are required to determine whether Fus3 phosphorylates additional GAPs and examine possible regulation of Rga2 by other MAPKs, including Hog1, whose activation is regulated by Cdc42 during the yeast response to hyperosmotic stress, a condition under which CN is also active (Chen and Thorner, 2007; Guiney *et al.*, 2015).

Regulation of Rho GAP activity is a fundamental mechanism to spatially and temporally regulate the dynamics of Rho GTPase signaling. In a fungal human pathogen, *Candida albicans*, phosphorylation and inhibition of Rga2 by a hyphal-specific Cdk are required for the morphogenetic switch from yeast to hyphal growth, which promotes virulence (Zheng *et al.*, 2007). Unidentified phosphatases may therefore prevent pathogenesis by maintaining the fungi in the yeast growth phase. In humans, epidermal growth factor promotes both phosphorylation and subsequent dephosphorylation of a Rho GAP, Deleted in Liver Cancer (DLC1), and disruption of this regulation increases cell spreading, which is linked to cell invasion and metastasis (Ravi *et al.*, 2015). Thus elucidating how and when Rho GAPs are controlled in vivo is a critical step toward unraveling the mechanisms that perturb Rho GTPase signaling to cause disease.

MATERIALS AND METHODS

Growth media and general methods

Yeast media and culturing methods were followed, as described, in synthetic complete medium (Sherman, 1991), except that twice the amount of amino acids and nucleotides was used. Yeast transformations were performed by the lithium acetate method (Ausubel *et al.*, 2001). Plasmids and yeast strains used in this study are listed in Supplemental Tables S1 and S2, respectively.

E. coli extract

For GST-peptide binding assays, plasmids for GST-Rga2 PxIxIT peptide (pNL118 and 120) or GST alone (pGEX4T-3) were transformed into BL21 DE3 cells (Invitrogen). Single colonies were grown in Luria broth supplemented with 50 µg/ml ampicillin overnight with shaking at 37°C. Overnight cultures were diluted to OD_{600} = 0.01 and grown with shaking at 37°C until OD_{600} = 0.5. Protein expression was induced with 1 mM isopropyl-β-D-thiogalactoside (IPTG) for 2 h with shaking at 37°C. Cultures were harvested by centrifugation (5 min, 5000 rpm at 4°C in a Sorvall GS-3 rotor). Pellets were washed in cold water and stored at −80°C. Pellets were resuspended in lysis buffer (50 mM Tris-HCl, pH 8, 100 mM NaCl, 2 mM ethylene glycol tetraacetic acid [EGTA], 2 mM EDTA, 5 mM dithiothreitol [DTT], protease inhibitors) and lysed by sonication 5 × 30 s at 30% output with 1-min breaks. Cold NaCl was immediately added to lysate to a final concentration of 1.5 M. Cell debris was pelleted (5 min, 10,000 rpm at 4°C in a Sorvall SS-34 rotor) and further clarified twice (20 min, 17,000 rpm at 4°C in a Sorvall SS-34 rotor). Tween-20 was added to clarified extracts to 0.1% final. Total protein concentration of extracts was determined by Bradford assay, and extracts were aliquoted and flash-frozen in liquid nitrogen and stored at −80°C.

For Rga2 full-length binding assays, His-Rga2 constructs (pNL143, 145,146) were transformed in BL21 DE3 cells (Invitrogen), and GST-CNA1 trunc + CNB1 was transformed in BL21 DE3 pLys cells (Invitrogen). Single colonies were grown in Luria broth supplemented with 50 µg/ml ampicillin overnight with shaking at 37°C. Overnight cultures were backdiluted to OD_{600} = 0.01 and grown with shaking at 37°C until OD_{600} = 0.5. Cultures were grown for an additional 1 h at 25°C and then induced with 1 mM IPTG at 18°C for 20 h. Cultures were harvested by centrifugation (5 min, 5000 rpm at 4°C using a Sorvall GS-3 rotor), flash-frozen in liquid nitrogen, and stored at −80°C. His-Rga2 pellets were lysed in lysis buffer (50 mM Tris-HCl, pH 7.5, 150 mM NaCl, 10% glycerol, 1 mM β-mercaptoethanol [β-ME], protease inhibitors) and sonicated 5 × 30 s at 30% output with 1-min breaks. GST-CNA1 and CNB1 pellets were lysed in lysis buffer (50 mM Tris-HCl, pH 8, 100 mM NaCl, 5 mM $MgCl_2$, 1 mM β-ME, and protease inhibitors) and sonicated 5 × 30 s at 30% output with 1-min breaks. Cell debris was pelleted (5 min, 10,000 rpm at 4°C in a Sorvall SS-34 rotor) and then clarified twice (20 min, 17,000 rpm at 4°C in a Sorvall SS-34 rotor). Total protein concentration of extracts was determined by Bradford assay, and extracts were aliquoted and flash-frozen in liquid nitrogen and stored at −80°C.

Purification of constitutively active truncated yeast CN

Plasmids for 6xHis-CN (CNA1trunc-p11) and Cnb1 (pET15b-Cnb1) were transformed into BL21 DE3 cells (Invitrogen). Single colonies were grown overnight in Luria broth supplemented with 50 µg/ml ampicillin with shaking at 37°C. Overnight cultures were diluted to OD_{600} = 0.01 in Luria broth supplemented with 100 µg/ml carbenicillin and 100 µg/ml kanamycin and grown with shaking at 37°C until OD_{600} = 0.5. Culture was grown for an additional 1 h with shaking at 25°C and then protein expression induced with 1 mM IPTG with shaking at 18°C for 20 h. Cultures were harvested by centrifugation (5 min, 5000 rpm at 4°C with a Sorvall GS-3 rotor), and pellets were washed in cold water and frozen at −80°C. Pellets were resuspended in lysis buffer (50 mM Tris-HCl, 150 mM NaCl, 1 mM β-ME, and protease inhibitors) and lysed by sonication: 5 × 30 s at 30% output with 1-min breaks. Cell debris was pelleted (5 min, 10,000 rpm at 4°C with a Sorvall SS-34 rotor) and further clarified twice (20 min, 17,000 rpm at 4°C with a Sorvall SS-34 rotor). CN complex was purified over a nickel–nitriloacetic acid (Ni-NTA) agarose column (FP2400000; 5 Prime) according to manufacturer's specifications. Purified protein was eluted in fractions with 150 mM imidazole and assayed by SDS–PAGE, pooled, and dialyzed into 50 mM Tris-HCl, pH 7.5, plus 100 mM NaCl buffer and stored at −80°C with 10% glycerol.

GST-peptide and CN trunc binding assay

To test the putative CN-docking site on Rga2, 50 µg of *E. coli* extract containing GST or GST-tagged peptide was mixed with 10 µg of purified 6xHis-CN trunc in binding buffer (50 mM Tris-HCl, pH 7.5,

150 mM NaCl, 0.1% Triton X-100, 1 mM β-ME, 5 mM imidazole) for 1 h at 4°C with end-over-end mixing. A 25-µl amount of washed Ni-NTA agarose beads (FP2400000; 5 Prime) was added to the binding mixture and incubated for another 2 h. Beads were washed three times in binding buffer containing 15 mM imidazole, and bound proteins were eluted by boiling in Laemmli buffer for 5 min. From 5 to 20 µl of sample was resolved by SDS–PAGE and immunoblotted with primary antibodies to GST (MMS112R500, mouse monoclonal; Covance/Berkeley Antibody Co.) and histidine (34660, mouse monoclonal; Qiagen). Primary antibodies were detected on film by chemiluminescence with secondary antibody α-mouse conjugated to horseradish peroxidase (NA931-1ML; GE Healthcare).

His-Rga2 and CN trunc binding assay

To test whether the CN-docking site is functional within the context of the full-length protein, 2.5 mg of *E. coli* extract containing 6xHis-tagged Rga2 was mixed with 30 µg of GST extract or 450 µg of GST-CNA1 trunc extract in binding buffer (50 mM Tris-HCl, pH 7.5, 150 mM NaCl, 0.1% Triton X-100, 1 mM β-ME, and protease inhibitors) for 1 h at 4°C with end-over-end mixing. A 25-µl amount of washed glutathione–Sepharose 4B beads (17075601; GE Healthcare) was added to the binding mixture and incubated for another 2 h. Beads were washed three times in binding buffer, and bound proteins were eluted by boiling in Laemmli buffer for 5 min. A 20-µl amount of sample was resolved by 10% acrylamide SDS–PAGE gel and immunoblotted with primary antibodies to GST (MMS112R500, mouse monoclonal; Covance) and histidine (34660, mouse monoclonal; Qiagen). Primary antibodies were detected by infrared (IR) fluorescence with secondary antibody anti-mouse conjugated to Alexa 680 (A-21058; Invitrogen) and visualized with an Odyssey scanner (Li-Cor Biosciences, Lincoln, NE).

Yeast extracts

For in vivo dephosphorylation under Ca^{2+}-activating conditions, cells at OD_{600} = 0.6 were treated with FK506 (1 µg/ml final concentration) or vehicle (90% ethanol and 10% Tween-20) for 30 min before protein induction with 2% galactose for 4 h. CN was then activated with 200 mM $CaCl_2$ for 20 min and then harvested with pellets stored at –80°C. Yeast pellets were resuspended in RIPA buffer (50 mM Tris-HCl, pH 7.4, 150 mM NaCl, 1 mM EDTA, 1% Triton X-100, 1 mM DTT, and protease inhibitors) and homogenized by glass-bead lysis on a vortexer, 5 × 2 min with 1-min breaks. Lysate was separated from beads by needle-puncture spin collection and further clarified at 14,000 rpm for 20 min. Total protein concentration of extracts was determined by Bradford assay. A 45-µg amount of total protein was analyzed by SDS–PAGE gel and immunoblotted with primary antibodies: anti-FLAG (F3165, mouse monoclonal; Sigma-Aldrich).

For experiments probing protein expression or phosphorylation state from yeast extracts, cultures were pelleted and washed with cold water before flash freezing in liquid nitrogen. Pellets were resuspended in urea lysis buffer (20 mM Tris-HCl, pH 7.5, 7 M urea, 2 M thiourea, 65 mM 3-[(3-cholamidopropyl)dimethylammonio]-1-propanesulfonate, 65 mM DTT, 50 mM NaF, 100 mM β-glycerophosphate, 1 mM $NaVO_3$, 1 mM phenylmethylsulfonyl fluoride) and homogenized by glass-bead lysis on a vortexer, 5 × 2 min, with 1-min break in between. Lysate was separated from beads by needle-puncture spin collection, and lysate was further clarified at 14,000 rpm for 10 min. Total protein concentration of extracts was determined by Bradford assay, and 30 µg of total protein was loaded to detect plasmid-expressed tagged-Rga2. For λ-phosphatase assay, yeast pellets were resuspended in RIPA buffer (50 mM Tris-HCl, pH 7.4, 150 mM NaCl, 1 mM EDTA, 1% Triton X-100, 1 mM DTT, and protease inhibitors) and homogenized by glass-bead lysis on a vortexer, 5 × 2 min with 1-min breaks. Lysate was separated from beads by needle-puncture spin collection and further clarified at 14,000 rpm for 20 min. Total protein concentration of extracts was determined by Bradford assay. Samples were analyzed by 5.5% acrylamide SDS–PAGE gel and immunoblotted with primary antibodies: anti-FLAG (sc-807, rabbit polyclonal, Santa Cruz Biotechnology; or F3165-1MG, mouse monoclonal, Sigma-Aldrich), anti-p44/42 MAPK (9101S, rabbit polyclonal; Cell Signaling Technologies), anti-Fus3 (sc-28548, rabbit polyclonal; Santa Cruz Biotechnology), and loading control, anti-Hsc82 (ab30920, rabbit polyclonal; Abcam). Primary antibodies were detected by IR fluorescence with secondary antibody anti-rabbit conjugated to Alexa 790 (A11369; Invitrogen) or anti-mouse conjugated to Alexa 680 (A-21058; Invitrogen) and visualized with an Odyssey scanner.

β-Galactosidase assay

YGS57 transformed with plasmids (pBA2059, pNL110-112) was grown in SC-LEU plus 2% raffinose to mid log phase, OD_{600} = 0.4. Rga2 expression was induced by adding 2% final galactose for 2 h. Cells were then backdiluted to OD_{600} = 0.5 and treated for 90 min with 5 µM α-factor (αF; RP01002; GenScript). A 100-µl amount of pheromone-treated cells was transferred to 96-well plates for FUS1-lacZ analysis, and 5-ml cultures were saved to assay Rga2 protein expression in yeast extracts as described. FUS1-lacZ activity was determined using substrate FDG (F-1179; Invitrogen) as previously described (Hoffman *et al*., 2002), and fluorescence emission at 530 nm was detected using a fluorescence plate reader (BioTEK, Winooski, VT). For FUS1-lacZ in the integrated strain, cells (NLY52 and 54) were grown in SCD to mid log phase, OD_{600} = 0.3, and treated for 90 min at indicated αF conditions. For Figure 4B, 15 or 16 biological samples over the course of 2 d for each $Rga2^{WT}$ and $Rga2^{AQALAA}$ were assayed for FUS1-lacZ activity. FUS1-lacZ activity was determined using as substrate fluorescein di-β-D-galactopyranoside and normalized to OD_{600}.

Yeast liquid growth assay

Yeast strain (NLY33) transformed with plasmids (pNL126-128, pNL135, or pEGKT) was grown in SCD-URA to mid log phase. Cells were then backdiluted to a starting OD_{600} = 0.01 in a 96-well plate and protein expression induced with 20 µM estradiol (E1024-1G; Sigma-Aldrich). Absorbance at 600 nm was read every 5 min for 24 h, and a growth rate of doubling/hour was calculated from at least three technical replicates. Data were analyzed by one-way analysis of variance (ANOVA) with Tukey's correction for multiple comparisons.

λ-Phosphatase treatment of Rga2 WT and PxIxIT mutant

Cells (NLY33) transformed with plasmids (pBA2059 or pNL111) were grown in SCD-LEU plus 5 nM estradiol to mid log phase. At OD_{600} = 0.35, cells were arrested in G1 with 10 µM αF for 2 h and then harvested. Yeast extracts were made in RIPA buffer as detailed earlier with 500 µg of total protein used to purify Rga2-FLAG by anti-FLAG immunoprecipitation. Protein-bound beads were washed with RIPA buffer and then washed into PMP buffer (50 mM 4-(2-hyd roxyethyl)-1-piperazineethanesulfonic acid [HEPES], 10 mM NaCl, 2 mM DTT, and 0.01% Brij 25). Beads were then incubated with 100–400 U of λ-protein phosphatase (P0753S; New England BioLabs) in PMP buffer supplemented with 1 mM $MgCl_2$ for 45 min at 30°C. For λ-phosphatase treatment in the presence of phosphatase inhibitors, a cocktail of sodium pyrophosphate (10 mM), sodium

fluoride (10 mM), sodium metavanadate (0.4 mM), sodium orthovanadate (0.4 mM), and 3-glycerol-phosphate (0.1 mM) was used. Proteins were eluted from beads by boiling in Laemmli buffer for 5 min. Samples were resolved by electrophoretic mobility in 5.5% acrylamide SDS–PAGE gel, and phosphorylation was assayed by immunoblot (anti-FLAG, rabbit) and Hsc82 loading control (anti-Hsc82). Primary antibody was detected by IR fluorescence with secondary antibody anti-rabbit conjugated to Alexa 790 (A11369; Invitrogen) and visualized with an Odyssey scanner. Percentage of total Rga2 signal represented by slower-migrating band was quantified by Image Studio (Li-Cor Biosciences).

In vivo kinase inhibition

Fus3-WT (NLY39+MR4937) or Fus3-as1 (NLY39+MR4938) was transformed with $Rga2^{WT}$-FLAG (pBA2059). Strains were grown in SCD-URA-LEU plus 5 nM estradiol at 30°C to OD_{600} = 0.3 before addition of 10 μM αF pheromone for 2 h, followed by addition of 10 μM 1Na-PP1 (10954; Cayman Chemical Company) or vehicle (dimethyl sulfoxide) for 10 min. Cells were harvested and processed as described in Hughes Hallett *et al.* (2014), and 30 μg of total protein was loaded to detect electrophoretic mobility by immunoblot. Samples were resolved by electrophoretic mobility in 5.5% acrylamide SDS–PAGE gel, and phosphorylation was assayed by immunoblot (anti-FLAG, mouse) and Hsc82 loading control (anti-Hsc82). Primary antibody was detected by IR fluorescence with secondary antibody anti-rabbit conjugated to Alexa 790 (A11369; Invitrogen) and visualized with an Odyssey. Percentage of total Rga2 signal represented by the slower-migrating band was quantified by Image Studio.

In vitro kinase assay

GST-Fus3 kinase was purified and assayed for in vitro activity as described in Parnell *et al.* (2005). Briefly, BL21 DE3 cells expressing pGEX-2T6-FUS3 or pGEX-2T6-FUS3 K42R were purified by glutathione–Sepharose (17075601, GE Healthcare). Rga2 constructs were purified by Ni-NTA in buffer (50 mM Tris-HCl, pH 7.5, 150 mM NaCl, 10% glycerol, 1 mM β-ME, protease inhibitors) from *E. coli* extracts prepared as described earlier. Approximately 100 nM $GST\text{-}Fus3^{WT}$ or $GST\text{-}Fus3^{K42R}$ was activated with 300 μM ATP in kinase buffer (25 mM HEPES, pH 7.2, 15 mM $MgCl_2$, 5 mM EGTA, 1 mM $MnCl_2$, 3.5 mM DTT, and protease inhibitors) before being incubated with 450 nM 6xHis-Rga2, $6xHis\text{-}Rga2^{AQALAA}$, or $6xHis\text{-}Rga2^{8A}$ supplemented with 5 μCi of [γ-^{32}P]ATP (PerkinElmer Cetus). Reaction was carried out at room temperature. Samples were collected at indicated time points and reaction terminated with addition of Laemmli buffer and boiling for 5 min. Samples were resolved in 7.5% SDS–PAGE, stained with Instant Blue Stain (Expedeon Protein Solutions), dried, and exposed to phosphoimager screen. The ^{32}P incorporation was detected with Typhoon scanner, and storage phosphor count signal was quantified using ImageJ (Schneider *et al.*, 2012) and normalized to Coomassie signal.

Pheromone time course

Cells (NLY33) transformed with plasmids (pBA2059 or pNL111) were grown in SCD-LEU plus 5 nM estradiol to mid log phase. At OD_{600} = 0.35, cells were treated with 0.2 M HU for 3 h and then washed and released into SCD-LEU plus 5 nM estradiol at $OD_{600} \approx 0.5$ and allowed to recover for 20 min before 10 μM αF was added at time 0. The 10-ml time points were taken every 15 min for fluorescence-activated cell sorting (FACS) analysis, microscopy, and electrophoretic mobility from yeast extracts prepared as described. A 35-μg amount of total protein was analyzed for electrophoretic mobility in 5.5% acrylamide SDS–PAGE gel, and phosphorylation was assayed by immunoblot (anti-FLAG, rabbit) and Hsc82 loading control (anti-Hsc82). Primary antibody was detected by IR fluorescence with secondary antibody anti-rabbit conjugated to Alexa 790 (A11369; Invitrogen) and visualized with an Odyssey scanner. Percentage of total Rga2 signal represented by the slower-migrating band was quantified by Image Studio.

Samples for Fus3 activation (phospho-Fus3) blot were resolved on 12% acrylamide SDS–PAGE gel and immunoblotted with primary antibodies anti-p44/42 MAPK and anti-Fus3. Primary antibodies were detected by IR fluorescence with secondary antibody anti-rabbit conjugated to Alexa 790 (A11369; Invitrogen) and visualized with an Odyssey scanner. Percentage of total Rga2 signal represented by the slower-migrating band was quantified by Image Studio.

FACS

A 1-ml amount of harvested yeast cells was fixed in 70% ethanol overnight at 4°C. Cells were washed in 50 mM sodium citrate, pH 7.4, sonicated briefly, and treated with 0.25 mg/ml RNase A for 2 h at 50°C and then 0.8 mg/ml Proteinase K for another 2 h at 50°C. Cells were washed in 50 mM sodium citrate before DNA was stained with 16 μg/ml propidium iodide in sodium citrate and analyzed on a BD FACS Calibur (BD Biosciences, San Jose, CA).

Microscopy

A 1-ml amount of harvested yeast cells was fixed in 70% ethanol overnight at 4°C. Cells were washed in 50 mM sodium citrate, pH 7.4, sonicated briefly, and stained with 24 mg/ml fluorescein isothiocyanate (FITC)–concanavalin A (C7642-2MG; Sigma-Aldrich) in P-buffer (10 mM sodium phosphate, 150 mM NaCl, pH 7.2) at room temperature for 5 min. Cells were washed in P-buffer and sonicated briefly before imaging with Zeiss Axio Imager M1 microscope (Carl Zeiss, Jena, Germany) with an LED lamp with a 100×/1.30 numerical aperture oil immersion objective. A 474/40-nm excitation and a 530/50-nm emission filter were used for FITC–concanavalin A imaging. Images were captured on a Hamamatsu Orca-ER digital camera (Bridgewater, NJ) coupled to Openlab Software 4.0.4 (PerkinElmer-Cetus).

ACKNOWLEDGMENTS

We thank Brenda Andrews, Henrik Dohlman, and Mark Rose for reagents and the members of the Cyert lab for helpful discussions and critical reading of the manuscript. We are grateful to Mardo Kõivomägi for his experimental guidance and support. We thank Pablo Aguilar for sharing unpublished data and for insightful discussion. Research reported here was supported by the National Institute of General Medical Services of the National Institutes of Health under Awards 5T32GM008412 and 2T32GM007276 to N.L. and R01GM48728 to M.S.C. The content is solely the responsibility of the authors and does not necessarily represent the official view of the National Institutes of Health.

REFERENCES

Abreu-Blanco MT, Verboon JM, Parkhurst SM (2014). Coordination of Rho family GTPase activities to orchestrate cytoskeleton responses during cell wound repair. Curr Biol 24, 144–155.

Alvaro CG, Aindow A, Thorner J (2016). Differential phosphorylation provides a switch to control how α-Arrestin Rod1 down-regulates mating pheromone response in saccharomyces cerevisiae. Genetics 203, 299–317.

Alvaro CG, O'Donnell AF, Prosser DC, Augustine AA, Goldman A, Brodsky JL, Cyert MS, Wendland B, Thorner J (2014). Specific α-arrestins negatively regulate Saccharomyces cerevisiae pheromone response by down-modulating the G-protein-coupled receptor Ste2. Mol Cell Biol 34, 2660–2681.
Alvaro CG, Thorner J (2016). Heterotrimeric G protein-coupled receptor signaling in yeast mating pheromone response. J Biol Chem 291, 7788–7795.
Arsenault HE, Roy J, Mapa CE, Cyert MS, Benanti JA (2015). Hcm1 integrates signals from Cdk1 and calcineurin to control cell proliferation. Mol Biol Cell 26, 3570–3577.
Ausubel FM, Brent R, Kingston RE, Moore DD, Seidman JG, Smith JA, Struhl K (2001). Current Protocols in Molecular Biology, Hoboken, NJ: John Wiley & Sons.
Bernards A, Settleman J (2004). GAP control: regulating the regulators of small GTPases. Trends Cell Biol 14, 377–385.
Bi E, Park H-O (2012). Cell polarization and cytokinesis in budding yeast. Genetics 191, 347–387.
Bidlingmaier S, Snyder M (2004). Regulation of polarized growth initiation and termination cycles by the polarisome and Cdc42 regulators. J Cell Biol 164, 207–218.
Bishop AC, Ubersax JA, Petsch DT, Matheos DP, Gray NS, Blethrow J, Shimizu E, Tsien JZ, Schultz PG, Rose MD, *et al*. (2000). A chemical switch for inhibitor-sensitive alleles of any protein kinase. Nature 407, 395–401.
Brand AC, Morrison E, Milne S, Gonia S, Gale CA, Gow NAR (2014). Cdc42 GTPase dynamics control directional growth responses. Proc Natl Acad Sci USA 111, 811–816.
Carbó N, Tarkowski N, Ipiña EP, Dawson SP, Aguilar PS (2017). Sexual pheromone modulates the frequency of cytosolic Ca^{2+} bursts in *Saccharomyces cerevisiae*. Mol Biol Cell 28, 501–510.
Caviston JP, Longtine M, Pringle JR, Bi E (2003). The role of Cdc42p GTPase-activating proteins in assembly of the septin ring in yeast. Mol Biol Cell 14, 4051–4066.
Chen GC, Zheng L, Chan CS (1996). The LIM domain-containing Dbm1 GTPase-activating protein is required for normal cellular morphogenesis in Saccharomyces cerevisiae. Mol Cell Biol 16, 1376–1390.
Chen J, Gutjahr C, Bleckmann A, Dresselhaus T (2015). Calcium signaling during reproduction and biotrophic fungal interactions in plants. Mol Plant 8, 595–611.
Chen RE, Thorner J (2007). Function and regulation in MAPK signaling pathways: lessons learned from the yeast Saccharomyces cerevisiae. Biochim Biophys Acta 1773, 1311–1340.
Chenevert J, Corrado K, Bender A, Pringle J, Herskowitz I (1992). A yeast gene (BEM1) necessary for cell polarization whose product contains two SH3 domains. Nature 356, 77–79.
Chenevert J, Valtz N, Herskowitz I (1994). Identification of genes required for normal pheromone-induced cell polarization in Saccharomyces cerevisiae. Genetics 136, 1287–1296.
Cherfils J (2014). GEFs and GAPs: mechanisms and structures. In: Ras Superfamily Small G Proteins: Biology and Mechanisms 1, Vienna: Springer, 51–63.
Clement ST, Dixit G, Dohlman HG (2013). Regulation of yeast G protein signaling by the kinases that activate the AMPK homolog Snf1. Sci Signal 6, ra78.
Crabtree GR, Schreiber SL (2009). SnapShot: Ca2+-calcineurin-NFAT signaling. Cell 138, 210–210.e1.
Cyert MS, Philpott CC (2013). Regulation of cation balance in Saccharomyces cerevisiae. Genetics 193, 677–713.
Cyert MS, Thorner J (1992). Regulatory subunit (CNB1 gene product) of yeast Ca2+/calmodulin-dependent phosphoprotein phosphatases is required for adaptation to pheromone. Mol Cell Biol 12, 3460–3469.
Elion EA, Satterberg B, Kranz JE (1993). FUS3 phosphorylates multiple components of the mating signal transduction cascade: evidence for STE12 and FAR1. Mol Biol Cell 4, 495–510.
Fritz RD, Pertz O (2016). The dynamics of spatio-temporal Rho GTPase signaling: formation of signaling patterns. F1000Res 5, 749.
Gao CY, Pinkham JL (2000). Tightly regulated, beta-estradiol dose-dependent expression system for yeast. Biotechniques 29, 1226–1231.
Ghaemmaghami S, Huh W-K, Bower K, Howson RW, Belle A, Dephoure N, O'Shea EK, Weissman JS (2003). Global analysis of protein expression in yeast. Nature 425, 737–741.
Goldman A, Roy J, Bodenmiller B, Wanka S, Landry CR, Aebersold R, Cyert MS (2014). The calcineurin signaling network evolves via conserved kinase-phosphatase modules that transcend substrate identity. Mol Cell 55, 422–435.
Grigoriu S, Bond R, Cossio P, Chen JA, Ly N, Hummer G, Page R, Cyert MS, Peti W (2013). The molecular mechanism of substrate engagement and immunosuppressant inhibition of calcineurin. PLoS Biol 11, e1001492.
Guiney EL, Goldman AR, Elias JE, Cyert MS (2015). Calcineurin regulates the yeast synaptojanin Inp53/Sjl3 during membrane stress. Mol Biol Cell 26, 769–785.
Hall A (2012). Rho family GTPases. Biochem Soc Trans 40, 1378–1382.
Hoffman GA, Garrison TR, Dohlman HG (2002). Analysis of RGS proteins in *Saccharomyces cerevisiae*. Methods Enzymol 344, 617–631.
Holowka D, Wilkes M, Stefan C, Baird B (2016). Roles for Ca2+ mobilization and its regulation in mast cell functions: recent progress. Biochem Soc Trans 44, 505–509.
Hughes Hallett JE, Luo X, Capaldi AP (2014). State transitions in the TORC1 signaling pathway and information processing in saccharomyces cerevisiae. Genetics 198, 773–786.
Iida H, Yagawa Y, Anraku Y (1990). Essential role for induced Ca2+ influx followed by [Ca2+]i rise in maintaining viability of yeast cells late in the mating pheromone response pathway. A study of [Ca2+]i in single Saccharomyces cerevisiae cells with imaging of fura-2. J Biol Chem 265, 13391–13399.
Ismael A, Tian W, Waszczak N, Wang X, Cao Y, Suchkov D, Bar E, Metodiev MV, Liang J, Arkowitz RA, *et al*. (2016). Gβ promotes pheromone receptor polarization and yeast chemotropism by inhibiting receptor phosphorylation. Sci Signal 9, ra38.
Juvvadi PR, Lamoth F, Steinbach WJ (2014). Calcineurin as a multifunctional regulator: unraveling novel functions in fungal stress responses, hyphal growth, drug resistance, and pathogenesis. Fungal Biol Rev 28, 56–69.
Knaus M, Pelli-Gulli M-P, van Drogen F, Springer S, Jaquenoud M, Peter M (2007). Phosphorylation of Bem2p and Bem3p may contribute to local activation of Cdc42p at bud emergence. EMBO J 26, 4501–4513.
Matheos D, Metodiev M, Muller E, Stone D, Rose MD (2004). Pheromone-induced polarization is dependent on the Fus3p MAPK acting through the formin Bni1p. J Cell Biol 165, 99–109.
McClure AW, Minakova M, Dyer JM, Zyla TR, Elston TC, Lew DJ (2015). Role of polarized G protein signaling in tracking pheromone gradients. Dev Cell 35, 471–482.
McCusker D, Denison C, Anderson S, Egelhofer TA, Yates JR, Gygi SP, Kellogg DR (2007). Cdk1 coordinates cell-surface growth with the cell cycle. Nat Cell Biol 9, 506–515.
Mócsai A, Walzog B, Lowell CA (2015). Intracellular signalling during neutrophil recruitment. Cardiovasc Res 107, 373–385.
Moser MJ, Geiser JR, Davis TN (1996). Ca2+-calmodulin promotes survival of pheromone-induced growth arrest by activation of calcineurin and Ca2+-calmodulin-dependent protein kinase. Mol Cell Biol 16, 4824–4831.
Narayanaswamy R, Moradi EK, Niu W, Hart GT, Davis M, McGary KL, Ellington AD, Marcotte EM (2009). Systematic definition of protein constituents along the major polarization axis reveals an adaptive reuse of the polarization machinery in pheromone-treated budding yeast. J Proteome Res 8, 6–19.
Nern A, Arkowitz RA (1999). A Cdc24p-Far1p-Gβγ protein complex required for yeast orientation during mating. J Cell Biol 144, 1187–1202.
Parnell SC, Marotti LA, Kiang L, Torres MP, Borchers CH, Dohlman HG (2005). Phosphorylation of the RGS protein Sst2 by the MAP kinase Fus3 and use of Sst2 as a model to analyze determinants of substrate sequence specificity. Biochemistry 44, 8159–8166.
Ravi A, Kaushik S, Ravichandran A, Pan CQ, Low BC (2015). Epidermal growth factor activates the Rho GTPase-activating protein (GAP) deleted in liver cancer 1 via focal adhesion kinase and protein phosphatase 2A. J Biol Chem 290, 4149–4162.
Roy J, Li H, Hogan PG, Cyert MS (2007). A conserved docking site modulates substrate affinity for calcineurin, signaling output, and in vivo function. Mol Cell 25, 889–901.
Rusnak F, Mertz P (2000). Calcineurin: form and function. Physiol Rev 80, 1483–1521.
Schneider CA, Rasband WS, Eliceiri KW (2012). NIH Image to ImageJ: 25 years of image analysis. Nat Methods 9, 671–675.
Sherman F (1991). Getting started with yeast. Methods Enzymol 194, 3–21.
Smith GR, Givan SA, Cullen P, Sprague GF (2002). GTPase-activating proteins for Cdc42. Eukaryot Cell 1, 469–480.
Sopko R, Huang D, Smith JC, Figeys D, Andrews BJ (2007). Activation of the Cdc42p GTPase by cyclin-dependent protein kinases in budding yeast. EMBO J 26, 4487–4500.

Stathopoulos AM, Cyert MS (1997). Calcineurin acts through the CRZ1/TCN1-encoded transcription factor to regulate gene expression in yeast. Genes Dev 11, 3432–3444.
Stevenson BJ, Ferguson B, De Virgilio C, Bi E, Pringle JR, Ammerer G, Sprague GF (1995). Mutation of RGA1, which encodes a putative GTPase-activating protein for the polarity-establishment protein Cdc42p, activates the pheromone-response pathway in the yeast Saccharomyces cerevisiae. Genes Dev 9, 2949–2963.
Sutherland DJ, Pujic Z, Goodhill GJ (2014). Calcium signaling in axon guidance. Trends Neurosci 37, 424–432.
Tedford K, Kim S, Sa D, Stevens K, Tyers M (1997). Regulation of the mating pheromone and invasive growth responses in yeast by two MAP kinase substrates. Curr Biol 7, 228–238.
Tong Z, Gao X-D, Howell AS, Bose I, Lew DJ, Bi E (2007). Adjacent positioning of cellular structures enabled by a Cdc42 GTPase-activating protein-mediated zone of inhibition. J Cell Biol 179, 1375–1384.
Veatch JR, McMurray MA, Nelson ZW, Gottschling DE (2009). Mitochondrial dysfunction leads to nuclear genome instability via an iron-sulfur cluster defect. Cell 137, 1247–1258.
Withee JL, Mulholland J, Jeng R, Cyert MS (1997). An essential role of the yeast pheromone-induced Ca2+ signal is to activate calcineurin. Mol Biol Cell 8, 263–277.
Zheng X-D, Lee RTH, Wang Y-M, Lin Q-S, Wang Y (2007). Phosphorylation of Rga2, a Cdc42 GAP, by CDK/Hgc1 is crucial for Candida albicans hyphal growth. EMBO J 26, 3760–3769.
Zheng Y, Cerione R, Bender A (1994). Control of the yeast bud-site assembly GTPase Cdc42. Catalysis of guanine nucleotide exchange by Cdc24 and stimulation of GTPase activity by Bem3. J Biol Chem 269, 2369–2372.
Zheng Y, Hart MJ, Shinjo K, Evans T, Bender A, Cerione RA (1993). Biochemical comparisons of the Saccharomyces cerevisiae Bem2 and Bem3 proteins. Delineation of a limit Cdc42 GTPase-activating protein domain. J Biol Chem 268, 24629–24634.